INVERSE METHOD FOR COMPRESSIVE STIFFNESS DETERMINATION OF IMPACT DAMAGE IN COMPOSITES

Pavel Sztefek and Robin Olsson

Imperial College London
Department of Aeronautics, London SW7 2AZ, UK
p.sztefek@imperial.ac.uk

ABSTRACT

This paper presents a non-contact optical method for determining the apparent in-plane stiffness reduction in the region of impact damage in composite laminates. The method is based on iterative updating of the material properties in a finite element model and its objective is to match the predicted displacement fields to those measured optically in impacted specimens under load. To examine the effect of the damage on buckling behaviour, the displacement fields obtained experimentally by digital image correlation are demonstrated and discussed. Finally, the method is applied to those measurements and the apparent stiffness of a real impact damage zone under the compressive load is evaluated.

1 INTRODUCTION

Impact is a serious concern for laminated composite structures, as impact damage may significantly reduce structural strength and stability [1]. The effect is particularly severe in compression, where impact may reduce the strength by up to 70% or more [1]. The effect of impact damage on global buckling is significantly smaller, but may still be appreciable [2]. In both cases knowledge of the constitutive properties in the damage zone is crucial for a reliable failure prediction.

Models for predicting strength after impact have been based on the concept of an equivalent hole [3] or soft inclusions, either uniform [4] or non-uniform [5]. Models have also been developed to consider how global buckling is affected by soft inclusions [6] and by inclusions in combination with local delamination buckling [7]. The main weakness of all these models is, however, lack of reliable experimental data to validate the assumed stiffness and its distribution in impact damage zones.

An initial study of the stiffness in impact damage zones was presented in [8], where coupons were cut from different locations in the damage zone and tested in tension and compression. The stiffness appeared to decrease towards the centre of the damage zone and reductions in tensile stiffness could be linked to a small central zone with fibre fracture. The main limitation of the method was that tests only could be done at low strains, as free edge effects and local buckling cause premature failure in narrow specimens. Furthermore, the approach only allowed a crude mapping of the local properties and required destruction of the laminate to be tested.

To eliminate these problems non-contact inverse methods have been developed. The present method uses iterative updating of the material properties in an FE model to match the displacements in the model to optically measured displacement fields in a damaged specimen under load. The approach was initially demonstrated on uniform soft inclusions in laminates [9]. After further development the method was used to determine non-uniform stiffness distributions in real impact damage under tension [10]. The damage zone was divided into a number of sub-regions with independent properties. A recent combined numerical and experimental study confirmed the link

between tensile stiffness reductions and fibre damage but also demonstrated that delaminations are significant in extending the zone influenced by fibre fracture [11]. An alternative inverse approach, based on direct calculation of the stiffness, has been used to determine flexural stiffness variations in impacted laminates [12].

The present study applies the inverse updating method presented in [10] to impact damage zones under compression, where delaminations cause local buckling of the damage zone even at low strains. The resulting surface strain variations are not representative of true variations in material membrane stiffness. For this reason the displacements in the damage zone have been discarded from the analysis. The damage zone is therefore represented by a uniform inclusion, which allows the apparent inclusion properties to be determined from the displacement field in the surrounding undamaged material.

2 INVERSE METHOD

2.1 Strategy

The inverse approach employing a Finite Element (FE) model updating technique was used in this paper to determine the apparent material properties of a damage region. The principle of FE model updating technique lies in iterative updating of the constitutive properties in an FE model, with the aim of minimising the difference between numerically predicted and experimentally measured displacement fields. The surface displacement fields of an impact damaged specimen are acquired during post-impact loading using an optical full-field method called Digital Image Correlation (DIC), also referred to as Digital Speckle Photogrammetry (DSP). FE predictions are conducted in the commercial package *ABAQUS*, where the updated displacement fields resulting from a specific set of material parameters are the product of interest. The fundamental idea of the inverse method is illustrated in Fig. 1.

The core elements of the inverse method are a gradient calculator and an optimization routine, which together perform a systematic search for a unique combination of the sought material properties. A gradient of the objective (displacement error) function determines whether to increase or decrease a particular material constant and serves as an input for the numerical optimizer. A modified first order optimization technique Steepest Descent is used in the current version of the inverse method [10]. This algorithm calculates how much a particular parameter should be changed. A schematic drawing of this optimization process is given in Fig. 2.

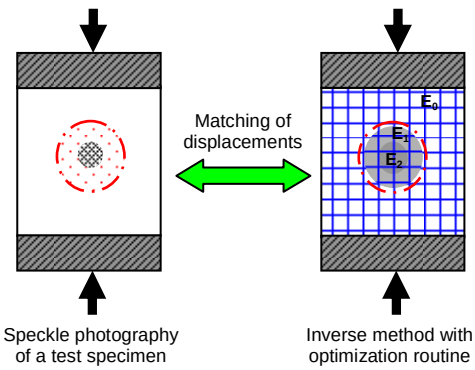

Fig. 1 Fundamental of the method

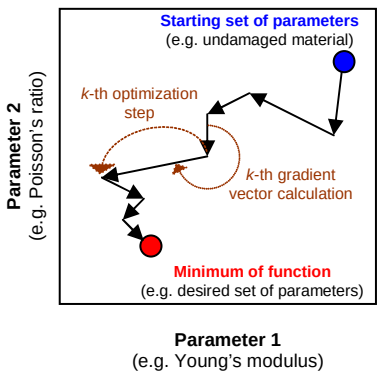

Fig. 2 Basic search procedure

The inverse method has first been numerically validated and then successfully applied on the results of post-impact tensile tests to obtain the local spatial stiffness distribution in impact damaged composite laminates [10]. Although the apparent average stiffness reduction in the damage zone rather than the material stiffness distribution is addressed in this paper, the same method can be used regardless of loading state of the specimen.

3 EXPERIMENTS

3.1 Specimens and Impacting

To study the stiffness of damage zones, 2.14 mm (16 ply) and 4.28 mm (32 ply) laminates were manufactured from Hexcel AS4/8552 carbon/epoxy prepreg with a cured ply thickness of approx. 0.133 mm. The lay-up of these quasi-isotropic laminates was $[(0/\pm45/90)_s/(90/\mp45/0)_s]_n$, where n = 1 or 2. Following the recommendations of the manufacturer, the panels were cured at 180°C and 100 psi for 2 h in the certified water-cooled autoclave. The compressive, homogenised, undamaged laminate properties were $E_x = E_y$ = 48.3 GPa, G_{xy} = 18.4 GPa and $\nu_{xy} = \nu_{yx}$ = 0.313. The specimens were initially cut into the dimension 150 × 100 mm, in order to fit into the modified compressive Boeing anti-buckling rig. Their size was further reduced to 148 × 100 mm resulting from grinding the loading edges of the specimen to assure their parallelism and thus a uniform far field load state. Prior to impacting the individual specimens were inspected for possible embedded defects using visual and ultrasonic (C-scan equipment) inspection and were found to be free of defects.

Use of a drop-weight machine featuring a 3.3 kg impactor with a hardened hemispherical steel tup of radius 6.35 mm provided appropriate impact damages at different energies. The specimens were clamped over a 125 × 75 mm opening by rubber covered toggle clamps which rendered approximately simply supported boundary conditions. The thin specimens were impacted at energies 2.5, 5 and 10 J and the thick specimens at energies 5, 10 and 20 J. After each impact, specimens were inspected by an Andscan ultrasonic scanning device. Since no delaminations were detected at the lowest energies, these specimens were subsequently impacted at 7 J for the thin specimens and 14 J for the thick specimens. All the energies after reimpacting resulted in Barely Visible Impact Damages (BVID).

3.2 Fractography

To determine the severity of the created damages, the ultrasonic C-scan system was used to inspect all the impacted specimens. Since time-of-flight measurements were not supported in the available software (i.e. the delamination depths could not be determined) additional investigations of the depth of the individual delaminations were carried out by the semi-automatic ultrasonic system Andscan. In addition, the spatial distribution of fibre fracture was observed after thermal deplying of the individual plies.

The fractographic findings are summarised in Fig. 3. The damages consisted of an approximately circular region with delaminations and central zones with various level of fibre fracture, always with a diameter of less than half of the delaminated area. Note that due to a lack of specimens, the distribution of fibre fracture was not evaluated for the thin specimen impacted at 10 J and for the thick specimen impacted at 20 J.

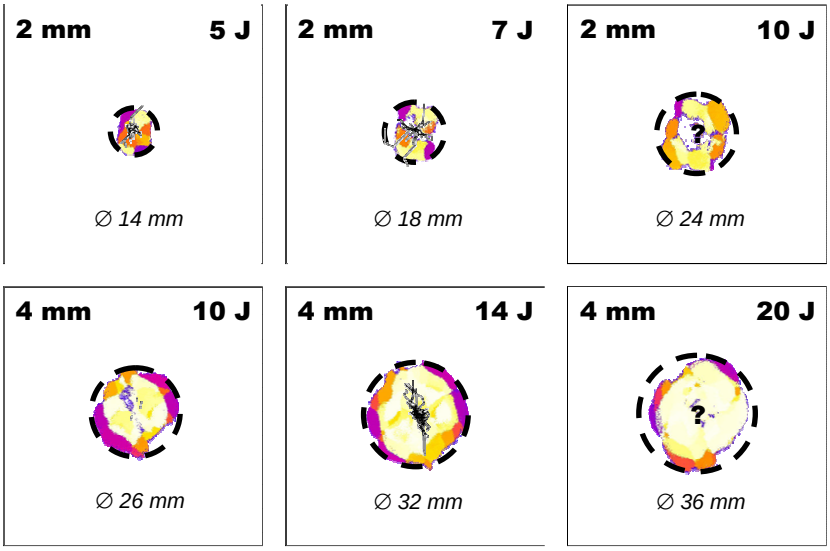

Fig. 3 The damage extension observed by fractographic techniques
("**?**" = unknown fibre damage)

3.3 Post-impact Loading

The impact damaged specimens were placed in a modified Boeing anti-buckling rig and loaded in compression, see Fig. 4. 3D full-field displacement maps were determined at certain load levels on both surfaces of the compressive specimens using the optical DIC system *ARAMIS*.

To be able to perform such measurements, a high contrast, speckle pattern was applied onto both sides of each specimen. A uniform layer of matt, black paint was sprayed onto the surfaces and this layer was then speckled with a matt, white spray paint.

The electromechanical, screw-driven 200 kN *ZWICK* machine was run in displacement control at rate of 1 mm/min until failure. The displacement and load signal of the *ZWICK* machine were recorded and in order to correlate the data with the DIC results, the load signal was also connected to the trigger box of the DIC system.

Despite using an anti-buckling rig, the specimens were expected to buckle out-of-plane under compressive load. Hence a stereo configuration of CCD cameras was used to capture that out-of-plane deformation. In total, two pairs of cameras were used simultaneously to map the displacements and deformations on both sides of the specimen. This setup allowed us to extract membrane and bending strains at any given time during loading and to observe local (delamination) buckling development on both sides.

An in-house setup procedure was implemented in order to centre, align and set the correct position of the two sets of cameras. This procedure involved using a thin perspex setup specimen designed by the authors. The identical characteristic features on the specimen were observed simultaneously by both sets of cameras and that allowed us to adjust the two pairs of cameras appropriately (i.e. symmetrically to the plane of the specimen) as illustrated in Fig. 5. This setup resulted in full-field measurements with a desired area and a desired orientation on both sides. The actual measuring area observed by both cameras was 100 × 80 mm. Synchronisation of the two pairs of cameras was guaranteed by running the DIC acquisition in a master-slave mode. The frame rate of cameras was set to 1 Hz.

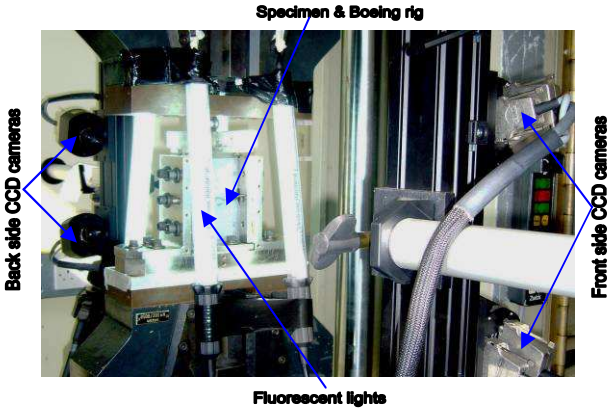

Fig. 4 Experimental setup

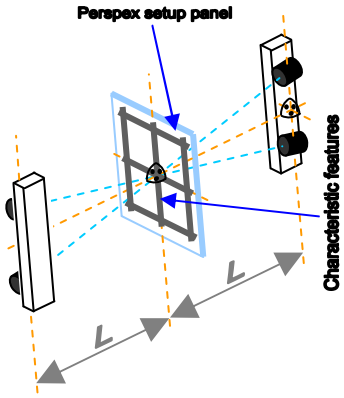

Fig. 5 Camera setup

Apart from the 2 mm specimen impacted at 5 J, all the tested specimens failed across the damage region, which indicates an effect of the impact damage on their compressive failure. The failure mode was dominated by the delamination buckling in association with the presence of initial imperfections (i.e. residual indentation after impact). Since the aim was to determine homogenised in-plane stiffness, applied strains were evaluated in the neutral surface, i.e. as the applied membrane strains. Failure values for the applied membrane strains and associated compressive load levels were between 0.57% (39.4 kN) and 0.65% (43.1 kN) for the 2 mm specimens and between 0.51% (89.5 kN) and 0.58% (105.9 kN) for the 4 mm specimens.

3.4 Observed Buckling Patterns

The failure of thin compressively loaded panels is driven by buckling behaviour. In impacted composite laminates, several types of buckling occur during loading, as shown in Fig. 6. Depending on the geometry and initial imperfections of the specimens, the severity of the impact damage and the boundary conditions during the test, these buckling types may happen either individually or interact with each other. It is important to understand how they interact (e.g. how the local delamination buckling affects the global response of the specimen, etc.) in order to understand how the damage affects the local stiffness of the impacted specimen.

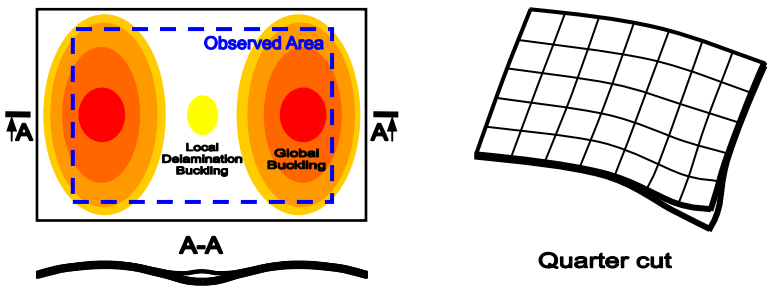

Fig. 6 Typical compressive response of an impacted plate

A comparison of buckling patterns within the observation area indicated in Fig. 6 at some applied membrane strain levels is given in Fig. 7. Note, that the full-field maps indicate the out-of-plane displacement on the impacted side of the specimen, while the associated graphs depict a longitudinal cross-section through the centre of impact damage on the front (blue) and back (red) surface. For the 2 mm specimens, there is a

change in the buckling mode from one to two buckles, observed around 0.3% of applied membrane strain. The buckling patterns at this strain level are therefore shown. The bottom displacement maps are shown at strain levels just before failure.

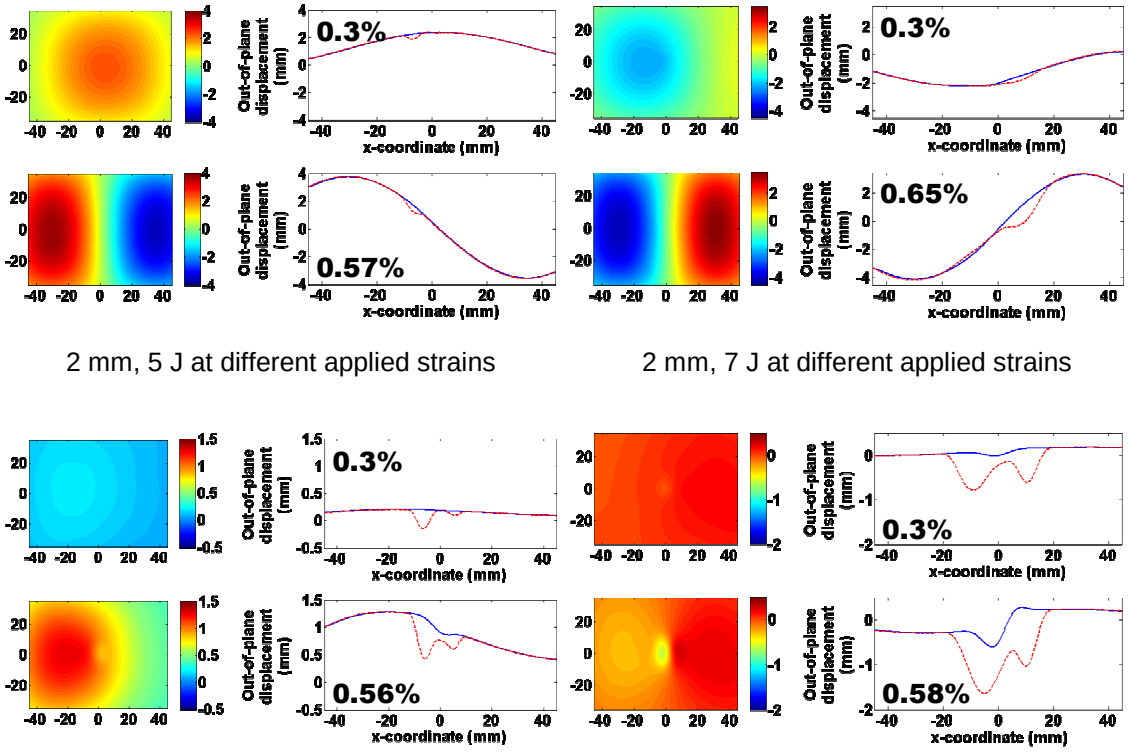

Fig. 7 Observed buckling patterns at strain of 0.3% and just before failure

At the damage location a strain concentration occurs, primarily due to local buckling. The effect of the impact damages caused by different energies is demonstrated in Fig. 8, which compares the concentration of strain in the loading direction on the impacted side, observed at 0.3% of applied membrane strain. It is noted that tensile strains occur on the edges of local buckles while compressive strains are located in the damage centre.

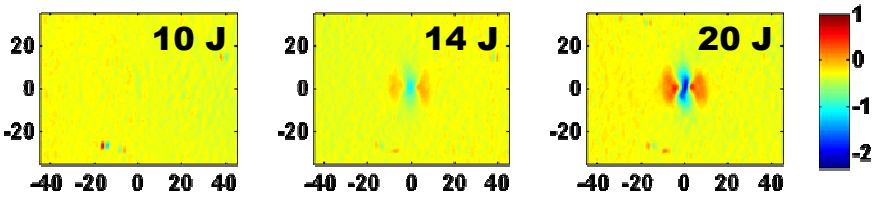

Fig. 8 Strain concentrations due to local buckling and fibre fracture in 4 mm specimens

4 STIFFNESS EVALUATION

Experimentally obtained displacement fields at certain load levels were used as an input for the inverse method. For the reconstruction of the nonlinear, apparent material characteristics, the displacement fields at applied membrane strains ranging from 0.05%

up to the failure with the increment of 0.05% were considered. The rectangular data matrices were extracted from the front and the back side of the tested laminates and transformed into a global coordinate system (x_G, y_G, z_G), see Fig. 9. The size of the area was 70 × 90 mm. Since the FE model used in the stiffness evaluation process consisted of shell elements, the experimental boundary conditions had to be obtained for the neutral surface of the specimen. Furthermore, as we were determining the in-plane material properties, only the membrane deformation was of concern to us.

While it is easy to separate membrane strains from bending strains, this operation is not as straight forward when dealing with displacement data. For this reason, it was decided to impose the bending as well as membrane boundary conditions onto the neutral surface of the FE model, as illustrated in Fig. 10. The boundary conditions of the FE model then consisted of full-field out-of-plane displacement constraints, representing the buckling behaviour of the specimen (note that the out-of-plane constraints are not applied in the delaminated region, the displacement readings of which are not representative of the specimen deformation – due to local buckling) and of in-plane displacement constraints imposed on the perimeter of the FE model simulating the loading conditions. This allowed us to examine the effect of the damage on the in-plane displacement components and to determine the apparent stiffness reduction within the delaminated region.

The term *apparent* stands for the fact that the determined stiffness reduction is not only related to the material degradation as such but is also affected by the local buckling of the delaminated area.

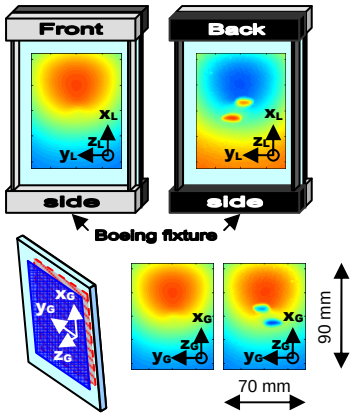

Fig. 9 Data extraction and transformation

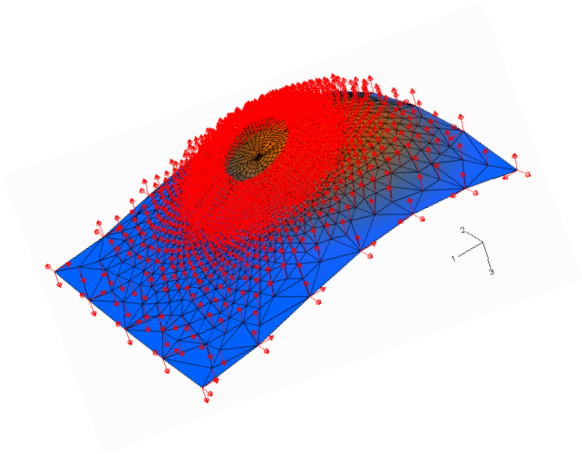

Fig. 10 FE model boundary conditions

The FE model used in the inverse procedure was a 70 × 90 mm 3D deformable model with linear, planar shell elements, using linear elastic material. The analysis was run in a geometrically nonlinear mode due to the relatively large displacements resulting from global buckling. The size of the nonlinear soft inclusion embedded in the modelled specimens was based on the envelope of the individual delaminated areas. As supported by C-scan and Andscan characterisations, the impact damages in our quasi-isotropic specimens were fairly circular and thus the nonlinear inclusions had circular geometries with diameter of 14 mm (5 J), 18 mm (7 J) and 24 mm (10 J) for the 2 mm models and 26 mm (10 J), 32 mm (14 J) and 36 mm (20 J) for the 4 mm models, as illustrated above in Fig. 3.

Having applied the inverse method to the results obtained at a certain applied membrane strain, a set of apparent material parameters was predicted in the inclusion region. Having run the method in the same fashion for different applied membrane strains, the load dependent histories of the constitutive parameters were evaluated in Fig 11. The resulting nonlinear material behaviour of the inclusion substituting a real impact damage was reconstructed as demonstrated in Fig. 12. It should be stressed that these nonlinear material curves were produced running a sequence of *ABAQUS* analyses with linear elastic material models.

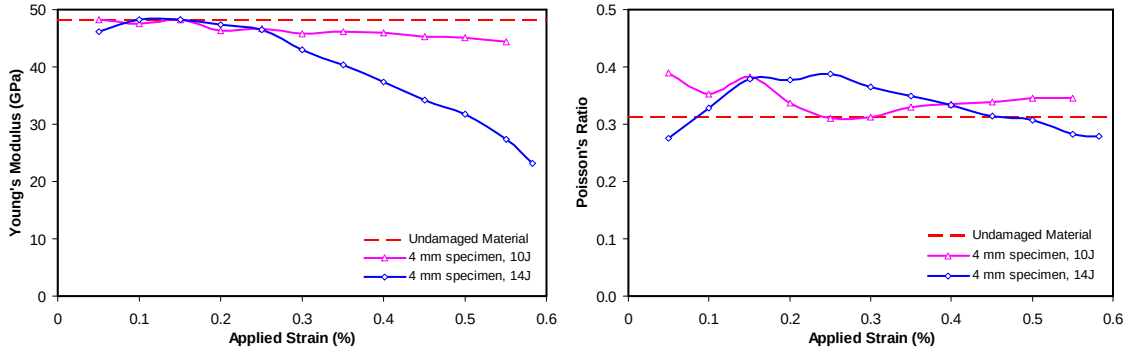

Fig. 11 Load dependent constitutive parameters of the damage region

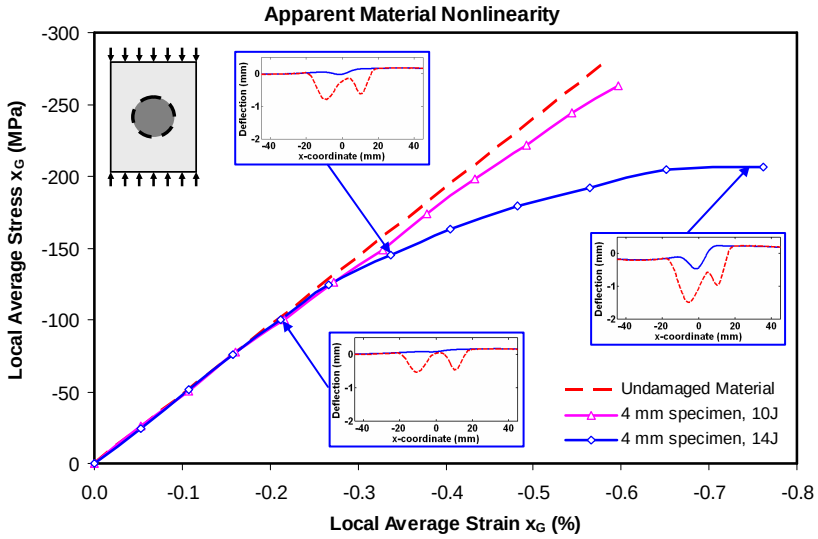

Fig. 12 Apparent, nonlinear material behaviour of the damage region

5 DISCUSSION

As opposed to tension, where the strain concentration is inherent predominantly due to fibre fracture, it was found in compression that local delamination buckling is the main cause for the strain amplitudes and distributions in impact damage zone; although the region with fibre failure contributes to additional local strain increase. Taking into account these aspects, it was vital to thoroughly describe the buckling behaviour of the specimens.

Measuring the full-field quantities on both surfaces of the tested specimens allowed us not only to separate membrane and flexural strains but also to track accurately the local

buckling development on each surface. Additional advantages of this setup are a precise description of initial imperfections introduced by manufacturing and impacting and in some special cases also capturing a rough growth of delaminations during loading.

The local delamination buckling influences the global buckling shape of the specimens as clearly demonstrated by buckling patterns in Fig. 7, in particular for 2 mm specimens. The specimen impacted at 5 J buckles initially in mode 1 with a symmetric half wave, whereas antisymmetric mode 1 is visible for the specimen impacted at 7 J. This is thought to be due to the larger delamination area and thus more extensive local buckling in the latter.

Relatively small local buckling is present in the 4 mm specimen impacted at 10 J. Since fractography revealed no fibre failure for this specimen/energy configuration, the apparent stiffness reduction is influenced merely by the delamination buckling. This is illustrated in Figs 11 and 12, in which the corresponding stiffness is only slightly lower than for the undamaged material. The nonlinear material curve for the 4 mm specimen impacted at 14 J shows much larger stiffness reduction, which is due to more pronounced local buckling combined with extensive fibre fracture, see Fig. 7. Both curves demonstrate a clear effect of local buckling on the apparent stiffness in delaminated area at approximately 0.2% of applied strain. The Poisson's effect is not entirely understood, however clear dependence on global buckling can be observed.

It should be elaborated upon the boundary conditions used in the FE model. In a buckled specimen, the in-plane displacements are affected by both the membrane shrinkage and the bending. To cancel the bending effect on the in-plane displacement, the out-of-plane constraints were applied to the whole FE model except the delaminated area to simulate the geometry of the specimen in a particular loading state. The in-plane boundary conditions of the edges of the FE model then imposed the membrane state in a particular loading state. This way, the only parameter influencing the in-plane displacement fields was the apparent stiffness of the delaminated region as desired.

6 CONCLUSIONS

An inverse method, previously developed by the authors for determining constitutive properties in damaged materials, has been applied to impact damage zones in laminates under compression.

Compression loading results in local delamination buckling of the damage zone, so that measured strain variations no longer correspond to true variations in material stiffness. For this reason no attempt was made to determine the spatial stiffness variation in the damage zone. Instead the damage was represented by a uniform inclusion, with *apparent* constitutive properties resulting from damage and local buckling. This causes an apparently nonlinear behaviour with a gradually decreasing stiffness, primarily due to increasing local buckling.

The delamination buckling observed on both sides of the laminated was shown to have an effect on forming the global buckling patterns.

An example of the apparent stress-strain behaviour has been given for a 4 mm thick laminate impacted at 10 J and 14J. The stress-strain curves were obtained by using the inverse method for a sequence of different applied strain levels, and it was found that changes in the apparent Young's modulus can be directly linked to local buckling events.

ACKNOWLEDGEMENTS

This project is funded by EPSRC in UK under grant EP/C531590/1. Parts of the experimental work were performed by visiting students Louise Belieres and Antoine Gamelin.

REFERENCES

1- Davies G.A.O., Olsson R., "Impact on composite structures", *The Aeron J*, 2004;108(1089):541-563.

2- Olsson R., "A review of impact experiments at FFA during 1986 to 1998", *FFA TN 1999-08*, 1999; Bromma: The Aeron Res Inst of Sweden.

3- Hawyes V.J., Curtis P.T., Soutis C., "Effect of impact damage on the compressive response of composites laminates", *Compos Part A: Appl Sci Manuf*, 2001;32(9):1263-1270.

4- Xiong Y., Poon C., Straznicky P.V., Vietinghoff H., "A prediction method for the compressive strength of impact damaged composite laminates", *Compos Struct*, 1995;30(4):357-367.

5- Nyman T., Bredberg A., Schön J., "Equivalent damage and residual strength for impact damaged composite structures", *J Reinf Plast Compos*, 2000;19(6):428-448.

6- Olsson R., Asp L.E., Nilsson S., Sjögren A., "A review of some key developments in the analysis of the effects of impact upon composite structures", *Composite Structures: Theory and Practice*, ASTM STP 1383. Grant P., Rousseau C., Eds; West Conshohocken: ASTM 2000:12-28.

7- Zeng L., Olsson R., "Buckling-induced delamination analysis of composite laminates with soft inclusion", *FOI-R-0412-SE*, 2002; Stockholm: Swedish Defence Research Agency.

8- Sjögren A., Krasnikovs Y., Varna J., "Experimental determination of elastic properties of impact damage in carbon fibre/epoxy laminates", *Compos Part A: Appl Sci Manuf*, 2001;32(9)1237-1242.

9- Olsson R., Iwarsson J., Melin L.G., Sjögren A., Solti J., "Experiments and analysis of laminates with artificial damage", *Compos Sci Technol*, 2003;63(2):199-209.

10- Sztefek P., Olsson R., "Tensile stiffness distribution in impacted composite laminates determined by an inverse method", *Compos Part A: Appl Sci Manuf*, doi:10.1016/j.compositesa.2007.10.005; In press.

11- Craven R., Sztefek P., Olsson R., "Investigation of impact damage in multi-directional tape laminates and its effect on local tensile stiffness", *Compos Sci Technol*, Under review.

12- Kim J.-H., Pierron F., Wisnom M.R., Syed-Muhamad K., "Identification of the local stiffness reduction of a damaged composite plate using the virtual fields method", *Compos Part A: Appl Sci Manuf*, 2007;38(9):2065-2075.